

# Bulk Entanglement and Boundary Spectra in Gapped Topological Phases

Zhu-Xi Luo,<sup>1</sup> Brendan G. Pankovich,<sup>1</sup> Yu-Ting Hu,<sup>2</sup> and Yong-Shi Wu<sup>3,4,5,1</sup>

<sup>1</sup>*Department of Physics and Astronomy, University of Utah, Salt Lake City, Utah, 84112, U.S.A.*

<sup>2</sup>*Department of Physics, Fudan University, Shanghai 200433, China*

<sup>3</sup>*Department of Physics and Center for Field Theory and Particle Physics, Fudan University, Shanghai 200433, China*

<sup>4</sup>*Key State Laboratory of Surface Physics, Fudan University, Shanghai 200433, China*

<sup>5</sup>*Collaborative Innovation Center of Advanced Microstructures, Fudan University, Shanghai 200433, China*

(Dated: November 4, 2018)

We study the correspondence between boundary spectrum of non-chiral topological orders on an open manifold  $\mathcal{M}$  with gapped boundaries and the entanglement spectrum in the bulk of gapped topological orders on a closed manifold. The closed manifold is bipartitioned into two subsystems, one of which has the same topology as  $\mathcal{M}$ . Specifically, we focus on the case of generalized string-net models and discuss the cases where  $\mathcal{M}$  is a disk or a cylinder. The correspondence turns out to be very different from that of the chiral topological orders. When  $\mathcal{M}$  has the topology of a cylinder, different boundary conditions of the cylinder will correspond to different entanglement cuts on the torus. Charge (smooth) and flux (rough) boundaries of toric code, more general  $\mathbb{Z}_N$  models, and the simplest non-abelian case of doubled Fibonacci are demonstrated.

## I. INTRODUCTION

Entanglement spectrum is the spectrum of entanglement Hamiltonian  $H_E$ , defined from the reduced density matrix of a bipartition of the system  $\rho_A = e^{-H_E}$ . It was introduced ten years ago by Li and Haldane [1] as an identification of topological order in fractional quantum Hall states. They showed that the state counting of low-lying entanglement spectrum of the model, e.g. those of the Laughlin and the Moore-Read states, is identical to the counting of conformal field theory modes describing low-energy boundary excitations.

Similar correspondence between bulk entanglement and boundary spectra has been studied analytically in various topological phases. For topological insulators, superconductors and general symmetry protected topological phases, degeneracies of bulk entanglement spectrum correspond to gapless edge modes [2–4]. For fractional quantum hall systems, rigorous results on a large class of trial wave functions have been obtained [5,6]. In Ref. [7], it was shown that the boundary conformal field theory (BCFT) and the bulk CFT used to construct the ground state trial wave function are isomorphic up to a Wick rotation. In general (2+1)d topological quantum systems possessing edge states described by a chiral (1+1)d CFT, a cut-and-glue method was applied in Ref. [8] to show that the reduced density matrix of a subregion in the bulk topological state is a thermal density matrix of the chiral edge state CFT that appear at the spatial boundary of the bulk subregion. Later a geometric proof was proposed [9].

Above methods can only be applied to chiral topological phases where there are chiral edge states appearing at boundaries of the system. In Ref. [10], the  $\mathbb{Z}_2$  spin liquid (toric code) model was discussed using free boundary conditions on a cylinder. An exact correspondence was found between the boundary and entanglement spectra. But it is yet to be clear how the three smooth-rough, rough-rough, smooth-smooth gapped boundary

conditions (in the sense of [15]) are related to the entanglement spectrum in the bulk. Recently Ref. [11] argues from an information-theoretical perspective that the entanglement spectrum of a subsystem is equal to the spectrum of a local thermal state living on the boundary of the subsystem. We would like to study the non-chiral version of the correspondence concretely in generalized string-net models with boundaries. String-net models [12] describe a large class non-chiral (2+1)d topological phases, including all those whose low-energy effective theories are discrete gauge or doubled Chern-Simons theories. The model was first constructed for closed manifolds but has been generalized to open manifolds for specific cases [13,14] and then generally formulated using module category [15,16]. Recently the explicit boundary Hamiltonian has been worked out using Frobenius algebras [17,18]. We will apply this formalism in the remaining of the paper, because it is more convenient for solving the spectrum and eigenstates.

Entanglement properties of string-net models were first discussed in [19] on a sphere. An universal constant term subleading to the area law was found and named as topological entanglement entropy. On nontrivial manifolds like a torus, the entanglement entropy turns out to be more complicated. In the case where the bipartition is done by cutting the torus into two cylinders, Ref. [20] carried out the calculation for toric code model, and subsequently defined the concept of minimally entangled states. Ref. [21] generalized them to minimally entangled sectors, which are classes of minimally entangled states that however be superposed, will always give the same entanglement entropy. In this work we focus on the correspondence between (1) boundary spectrum of string-net model on an open manifold (2) the entanglement spectrum obtained from bipartitioning a closed manifold into two subsystems  $A, B$  so that subsystem  $A$  has the same topology of the open manifold where the boundary spectrum is calculated.

In section II, we review the construction of string-net

model on open systems using Frobenius algebras. Section III demonstrates the correspondence in the case of a boundary spectrum for a disk and the entanglement spectrum for a disk-shaped subsystem. Simple examples of toric code and doubled Fibonacci models are presented. Then in IV we study the correspondence for boundary spectrum on a cylinder and entanglement spectrum for a torus bipartitioned into a cylindrical subsystem  $A$  and the rest, using the example of toric code [23]. Each of the three different possible boundary conditions of the toric code model on a cylinder correspond to an entanglement spectrum on a torus with different cuts, made possible through the introduction of minimally entangled sectors.  $\mathbb{Z}_N$  models are also demonstrated. Finally in V we discuss the cylinder-torus correspondence of non-abelian models using the doubled Fibonacci example and comment on subtleties arising from the most general cases.

## II. STRING-NET MODEL WITH BOUNDARIES

We briefly review the general theory of string-net model on manifolds with boundaries following [17,18]. Typical examples will be presented in the latter sections.

The input data  $\{I, d, \delta, G\}$  in the bulk of string-net models form a unitary fusion category  $\mathcal{C}$ . The model is defined on a trivalent graph on a closed oriented surface. Degrees of freedom live on links of the graph. For each link, we assign a string type  $j \in I = \{j = 0, 1, \dots, N\}$ , where  $I$  is called the label set. In the case of lattice gauge theories,  $j$ 's label the irreducible representations of a group. More generally, they can label irreducible representations of quantum groups. The Hilbert space is spanned by all configurations of the labels on links. Each label  $j$  has a ‘‘conjugate’’  $j^* \in I$ , satisfying  $j^{**} = j$ . There is unique ‘‘vacuum’’ label  $j = 0$  with  $0^* = 0$ . We require the state to be the same if one reverses the direction of one link and replaces the label  $j$  by  $j^*$ , which is a graphical realization of time reversal symmetry.

We associate to each string type a number  $d_j$  called quantum dimension of  $j$ , and define the total quantum dimension to be  $D = \sum_{j \in I} d_j^2$ . We further assign to each three string types a tensor  $\delta_{ijk}$  which specifies the branching rules of a trivalent graph. If for some  $i, j, k \in I$  one has  $\delta_{ijk} = 1$ , then the three string types are allowed to meet at a vertex. Otherwise their meeting is not energetically favored, i.e., we will have charge excitations on the corresponding vertex. (We will focus on the multiplicity-free cases for convenience.)

Given the quantum dimensions and fusion rules, we define the symmetrized  $6j$ -symbols, often denoted as  $G$ . They are complex numbers satisfying the following conditions [39]:

$$\begin{aligned} G_{klm}^{ijm} &= G_{nk^*l^*}^{mij} = G_{ijn^*}^{klm^*} = \iota_m \iota_n \overline{G_{l^*k^*n^*}^{j^*i^*m^*}}, \\ \sum_n d_n G_{kp^*n}^{mlq} G_{mns^*}^{jip} G_{lkr^*}^{js^*n} &= G_{q^*kr^*}^{jip} G_{mls^*}^{rjq^*}, \\ \sum_n d_n G_{kp^*n}^{mlq} G_{pk^*n}^{l^*m^*i^*} &= \frac{\delta_{iq}}{d_i} \delta_{mlq} \delta_{k^*ip}, \end{aligned} \quad (1)$$

where the first condition specifies tetrahedral symmetry, the second the pentagon identity, and the third orthogonality condition. The number  $\iota_j$  is the Frobenius-Schur indicator. In the example of lattice gauge theories, this indicator tells whether the representation  $j$  is real, complex, or pseudoreal. Then  $d_j = \iota_j \dim(j)$  with  $\dim(j)$  being the corresponding dimension of the space of the representation  $j$ ; and the tensor  $G_{klm}^{ijm}$  is the (symmetrized) Racah  $6j$  symbol for the group. In this example, string-net model can be mapped to the Kitaev's quantum double model.

Two types of local operators are needed to specify the Hamiltonian. On every vertex  $v$ , we have  $Q_v = \delta_{ijk}$  that acts on the labels of three edges incoming to the vertex  $v$ . On every plaquette  $p$ , we have  $B_p^s$  with  $s \in I$ , which acts on the boundary edges of the plaquette  $p$ . Its matrix elements on a triangular plaquette is [39],

$$\begin{aligned} \left\langle \begin{array}{c} j_5 \quad j_3 \quad j_6 \\ \swarrow \quad \downarrow \quad \searrow \\ j_1 \quad j_2 \quad j_4 \end{array} \middle| B_p^s \middle| \begin{array}{c} j_5 \quad j_3 \quad j_6 \\ \swarrow \quad \downarrow \quad \searrow \\ j_1 \quad j_2 \quad j_4 \end{array} \right\rangle \\ = v_{j_1} v_{j_2} v_{j_3} v_{j_1^*} v_{j_2^*} v_{j_3^*} G_{s j_3^* j_1^*}^{j_5 j_1^* j_3} G_{s j_1^* j_2^*}^{j_4 j_2^* j_1} G_{s j_2^* j_3^*}^{j_6 j_3^* j_2}, \end{aligned} \quad (2)$$

where  $v_j = \sqrt{d_j} = \frac{1}{G_{00j}^{j^*0j}}$ . The same pattern for  $B_p^s$  applies when the plaquette  $p$  is a quadrangle, a pentagon, etc..

Defining  $B_p = \frac{1}{D} \sum_s d_s B_p^s$ , the operators  $Q_v$ 's and  $B_p$ 's are mutually-commuting. Furthermore, they are also projectors:  $Q_v^2 = Q_v$  and  $B_p^2 = B_p$ . The Hamiltonian of the model is

$$H_{\text{bulk}} = \sum_v (1 - Q_v) + \sum_p (1 - B_p), \quad (3)$$

where the sum runs over vertices  $v$  and plaquettes  $p$  of the whole trivalent graph. Because of the commutative property of  $Q_v$  and  $B_p$ 's, the Hamiltonian is exactly soluble. Ground states satisfies  $Q_v = B_p = 1$  for all  $v, p$ .

The bulk ground states are invariant under any composition of the following elementary (dual) Pachner moves:

$$\begin{aligned} T_{2 \rightarrow 2} \left| \begin{array}{c} j_4 \\ \swarrow \quad \downarrow \quad \searrow \\ j_1 \quad j_2 \quad j_3 \end{array} \right\rangle &= \sum_{j_5} G_{j_3 j_4 j_5}^{j_1 j_2 j_5} v_{j_5} v_{j_5^*} \left| \begin{array}{c} j_4 \\ \swarrow \quad \downarrow \quad \searrow \\ j_1 \quad j_2 \quad j_3 \end{array} \right\rangle \\ T_{1 \rightarrow 3} \left| \begin{array}{c} j_3 \\ \swarrow \quad \downarrow \\ j_1 \quad j_2 \end{array} \right\rangle &= \sum_{j_4, j_5, j_6} \frac{v_{j_5} v_{j_6} v_{j_4}}{\sqrt{D}} G_{j_5 j_6 j_4}^{j_1 j_2 j_3} \left| \begin{array}{c} j_6 \\ \swarrow \quad \downarrow \quad \searrow \\ j_1 \quad j_4 \quad j_5 \end{array} \right\rangle \\ T_{3 \rightarrow 1} \left| \begin{array}{c} j_6 \\ \swarrow \quad \downarrow \quad \searrow \\ j_1 \quad j_4 \quad j_5 \end{array} \right\rangle &= \frac{v_{j_5} v_{j_4} v_{j_6}}{\sqrt{D}} G_{j_5 j_4 j_6}^{j_1 j_3 j_2^*} \left| \begin{array}{c} j_3 \\ \swarrow \quad \downarrow \\ j_1 \quad j_2 \end{array} \right\rangle \end{aligned}$$

The boundary theory of string-net models was first formulated in an abstract language by Ref. [15,16], building on the module category  $\mathcal{M}$  of the input category  $\mathcal{C}$ . An alternative was developed in Ref. [17,18], where the

Hamiltonian is written explicitly in terms of input data and can be used to solve for the spectrum and eigenstates. The basic object in this formulation is a separable Frobenius algebra  $\mathcal{A}$  constructed from  $\mathcal{C}$  and the boundary degrees of freedom form modules of the algebra. These two formulations [15,17] are mathematically equivalent due to a theorem: the category of right modules over an algebra  $\mathcal{A}$  is equivalent to the right module category  $\mathcal{M}$  over (unitary fusion)  $\mathcal{C}$  [24].

A Frobenius algebra is the subset  $I_{\mathcal{A}} \subset I$  equipped with a multiplication structure  $f_{ijk}$  which describes the fusion of open links  $i \otimes j \rightarrow k^*$  and satisfies the following constraints:

$$\text{Association: } \sum_c f_{abc^*} f_{cde^*} G_{de^*g}^{abc^*} v_c v_g = f_{age^*} f_{bdg^*}, \quad (4)$$

$$\text{Non-degeneracy } f_{aa^*0} \neq 0, \forall a \in I_{\mathcal{A}}.$$

We choose to normalize as  $f_{aa^*0} = 1 \forall a \in I_{\mathcal{A}}$ . There are two types of boundary degrees of freedom:  $l \in I$  on the wall and  $a \in I_{\mathcal{A}}$  on the open links, as indicated in Fig.1.

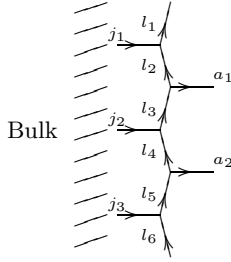


FIG. 1: Boundary is a wall carrying open links. Degrees of freedom on the wall are labeled by  $l \in I$ , and open links by  $a \in I_{\mathcal{A}}$ .

The boundary Hamiltonian can then be defined using the Frobenius algebra:

$$H_{\text{bdry}} = \sum_n (1 - \bar{Q}_n) + \sum_n (1 - \bar{B}_p), \quad (5)$$

with  $\bar{Q}_n$  acting on the open link  $n$  and projecting the boundary degrees of freedom to  $I_{\mathcal{A}}$ :

$$\bar{Q}_n \left| \begin{array}{c} j_2 \\ \leftarrow a_n \\ j_1 \end{array} \right\rangle = \delta_{a_n \in I_{\mathcal{A}}} \left| \begin{array}{c} j_2 \\ \leftarrow a_n \\ j_1 \end{array} \right\rangle. \quad (6)$$

$\bar{B}_p$  is a combination of  $\bar{B}_p^t$ 's,

$$\bar{B}_p = \frac{1}{d_{\mathcal{A}}} \sum_{t \in I_{\mathcal{A}}} \bar{B}_p^t, \quad d_{\mathcal{A}} = \sum_{t \in I_{\mathcal{A}}} d_t. \quad (7)$$

The operator  $\bar{B}_p^t$  fuses a string  $t$  to the boundary ‘‘half

plaquette’’ as follows:

$$\bar{B}_p^t : \left| \begin{array}{c} j_4 \\ \leftarrow a_2 \\ j_3 \\ \leftarrow a_2 \\ j_2 \\ \leftarrow a_1 \\ j_1 \end{array} \right\rangle \mapsto \sum_{a'_1, a'_2, j'_2, j'_3} f_{t^* a'_2^* a_2} f_{a_1 t a'_1^*} u_{a_1} u_{a_2} u_{a'_1} \\ \times u_{a'_2} G_{t^* a'_2^* j'_3}^{j_4^* j_3^* a_2^*} G_{t^* j'_3^* j'_2}^{j_5^* j_2^* j_3^*} G_{j_1 a_1^* a'_1}^{t^* j_2^* j_2} v_{j_2} v_{j_3} v_{j'_2} v_{j'_3} \left| \begin{array}{c} j_4 \\ \leftarrow a_2 \\ j_3 \\ \leftarrow a_2 \\ j_2 \\ \leftarrow a_1 \\ j_1 \end{array} \right\rangle. \quad (8)$$

One can easily check that the boundary plaquette operators are mutual commuting projection operators and they commute with the bulk operators. The full Hamiltonian of the system will then be

$$H = H_{\text{bulk}} + \epsilon H_{\text{bdry}}, \quad (9)$$

with  $\epsilon$  a small number due to the requirement for the system to be large.

Similar to the elementary Pachner moves in the bulk (4), one can use the Frobenius algebra  $\mathcal{A}$  to define transformations associated with on the boundaries of a graph. The ground states of string-net models with boundaries are invariant under the following elementary moves:

$$T_{1 \rightarrow 2} \left| \begin{array}{c} j \\ \leftarrow a_1 \\ i \end{array} \right\rangle = \sum_{a_2, a_3} \frac{u_{a_1} u_{a_2} u_{a_3}}{\sqrt{d_{\mathcal{A}}}} \sum_k v_k f_{a_2^* a_3^* a_1} G_{a_2^* a_3^* k}^{j^* i a_1^*} \left| \begin{array}{c} j \\ \leftarrow a_3 \\ k \\ \leftarrow a_2 \\ i \end{array} \right\rangle, \\ T_{2 \rightarrow 1} \left| \begin{array}{c} j \\ \leftarrow a_3 \\ k \\ \leftarrow a_2 \\ i \end{array} \right\rangle = \sum_{a_1} \frac{u_{a_1} u_{a_2} u_{a_3}}{\sqrt{d_{\mathcal{A}}}} v_k f_{a_2 a_3 a_1^*} G_{a_2^* k^* a_3}^{j a_1 i^*} \left| \begin{array}{c} j \\ \leftarrow a_1 \\ i \end{array} \right\rangle.$$

where  $u_a = \sqrt{v_a}$ .

For any input data in the bulk, there is always a trivial Frobenius algebra  $\mathcal{A}_0$  corresponding to  $I_{\mathcal{A}} = \{0\}$ . This is often called the ‘‘smooth’’ boundary in literature, but we will use instead the term ‘‘charge boundary’’ instead because in this case the boundary Hamiltonian reduces to the charge term only,  $H_{\text{bdry}}^{\text{charge}} = -\sum_n (1 - \bar{Q}_n)$ . On the other hand, the ‘‘rough’’ or ‘‘flux’’ boundaries  $I_{\mathcal{A}} = I$  are not guaranteed to exist for general string-net models. However, they do appear in important examples like the toric code and the doubled Fibonacci model, which will be discussed in latter sections. When exist, they Hamiltonian is simply  $H_{\text{bdry}}^{\text{flux}} = -\sum_n (1 - \bar{B}_p)$ .

For the case of a disk, if a flux/rough boundary exist for a set of input data, then the  $\bar{B}_p$  terms reduce to  $\bar{B}_{n, n+1}$  where the half plaquette  $\bar{B}_p$  lies between the open links  $a_n$  and  $a_{n+1}$ . Specifically, the matrix elements are given

by

$$\begin{aligned}
 & \left\langle \begin{array}{c} l_{n+1} \\ \leftarrow a'_{n+1} \\ l'_n \\ \leftarrow a'_n \\ l_{n-1} \end{array} \middle| \overline{B}^t_{(n,n+1)} \middle| \begin{array}{c} l_{n+1} \\ \leftarrow a_{n+1} \\ l_n \\ \leftarrow a_n \\ l_{n-1} \end{array} \right\rangle \\
 &= u_{a_n} u_{a_{n+1}} u_{a'_n} u_{a'_{n+1}} v_{l_n} v_{l'_n} f_{a_{n+1} l'_n a'_n} f_{l_n a_{n+1} a'_n} \\
 & \quad \times G_{l'_n a'_{n+1} l'_n}^{l_{n+1} a_{n+1}} G_{a'_n l'_n a'_n}^{l_n a_n}.
 \end{aligned} \tag{10}$$

The ground state is  $GSD_{D^2}^{\text{flux}} = \text{tr} (B_p \prod_n \overline{B}_{n,n+1}) = 1$ .

### III. THE CORRESPONDENCE FOR A DISK

#### A. Boundary spectrum on a disk

The ground state is always non-degenerate on a disk. Throughout the paper we assume the bulk is in its ground state, which is guaranteed by the small parameter  $\epsilon$  in equation (9). The  $n$ -th excited state of the full system then corresponds to  $n$  total boundary excitations created from the ground state. If there are  $n_\alpha$  boundary excitations of type  $\alpha$ ,  $n_\beta$  of type  $\beta$  etc., the degeneracy for this excited state then includes the number of possible distributions of these boundary excitations on these sites:

$$\binom{L}{n_\alpha} \binom{L-n_\alpha}{n_\beta} \binom{L-n_\alpha-n_\beta}{n_\gamma} \dots \binom{n_\zeta}{n_\zeta},$$

satisfying  $n = n_\alpha + n_\beta + \dots$ ,  $n \leq L$ . Since these excitations are created from the ground state, they should conversely fuse into vacuum. Labeling the number of fusion channels as  $g_n$ , the degeneracy at level  $n$  is

$$\begin{aligned}
 \text{deg}_n(D^2) &= \sum_{\{n_\alpha\}} g_n \binom{L}{n_\alpha} \binom{L-n_\alpha}{n_\beta} \\
 & \quad \times \binom{L-n_\alpha-n_\beta}{n_\gamma} \dots \binom{n_\zeta}{n_\zeta}.
 \end{aligned} \tag{11}$$

Here the sum over  $\{n_\alpha\}$  means to sum over all combinations  $\{n_\alpha, n_\beta, \dots, n_\zeta\}$  subject to the constraint  $n_\alpha + n_\beta + \dots + n_\zeta = n$ . Specifically for a charge/smooth boundary, the boundary excitations are all charges, while for a flux/rough boundary (if exists), they are all fluxes.

#### B. Entanglement spectrum for a disk subsystem

Now we turn to the reduced density matrix obtained from putting a string-net ground state on  $S^2$ , bipartitioning it into two disks  $A, B$ , and tracing out one of them. For convenience, we specify the cut to be of rough type, namely, the cut intersects links instead of passing through vertices; the latter type of cut will give no physical difference. The remaining disk  $A$  can be smoothly deformed into the following configuration 2.

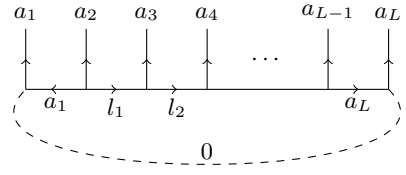


FIG. 2: Basic tree-like configuration in a disk-shaped region  $A$ .

Such a reduced density matrix was calculated in [19],

$$\langle \{a', l'\} | \rho_A | \{a, l\} \rangle = \delta_{\{a\}, \{a'\}} \delta_{\{l\}, \{l'\}} \prod_{m=1}^L \frac{d_{a_m}}{D^{L-1}}. \tag{12}$$

To make a connection with the boundary spectrum discussed in the last section III A, one can recast the above formula (12) using fiber fusion category language developed in [21], as

$$\rho_A = DP_0(\alpha^{\otimes L}), \tag{13}$$

where  $\alpha$  is a diagonal matrix with rank  $|I|$ , the number of string types in the input category. The entries are  $\alpha_j = d_j/D$ . We define a product “ $\otimes$ ” for  $\alpha$  as

$$\alpha_k^{\otimes 2} = (\alpha \otimes \alpha)_k = \oplus_{i,j \in I} \alpha_i \alpha_j \delta_{jik^*}. \tag{14}$$

The resultant  $\alpha^{\otimes 2}$  is again a diagonal matrix, and generally one has

$$\alpha_k^{\otimes L} = (\alpha^{\otimes(L-1)} \otimes \alpha)_k = \oplus_{i,j \in I} \alpha_i^{\otimes(L-1)} \alpha_j \delta_{ijk^*}. \tag{15}$$

Operator  $P_j$  projects onto the  $j$ -component of the  $\alpha^{\otimes L}$  matrix, so that  $P_0$  implements the constraint that all open links should fuse to vacuum.

Suppose the nontrivial open links with label  $a \neq 0$  appears  $n_a$  times in the configuration  $\{a_1, a_2, \dots, a_L\}$  of 2, so that the total number of nontrivial open links is  $n = \sum_{a \neq 0} n_a$ . The diagonal reduced density matrix  $\rho_A$  in (13) then consists of blocks of smaller diagonal matrices

$$\rho_A = \oplus_n \rho_{(A,n)} = \oplus_n \oplus_{\{a_n\}} \rho_{(A,n,\{a_n\})}, \tag{16}$$

with the direct sum over  $\{a_n\}$  subject to the constraint  $n = \sum_{a \neq 0} n_a$ . Then the dimension of each  $\rho_{(A,n)}$  is exactly equal to  $\text{deg}_n(D^2)$  in (11). So there is a one-to-one correspondence between the entanglement spectrum for a sphere and the energy spectrum for a disk.

In the above discussions, we have taken  $\alpha$  to be a diagonal matrix with rank  $|I|$ , which implies that the corresponding boundary theory is of charge/smooth type. Namely, the boundary excitations  $n_\alpha, n_\beta, \dots, n_\zeta$  are all charges. More generally for a boundary theory with Frobenius algebra  $I_A \subsetneq I$ , it is tempting to take  $\alpha$  to be of rank  $|I_A|$ , where each  $\alpha_j = d_j/d_A$  has  $j \in I_A$ . However at this moment it is not clear what the physical meaning is, to constrain the open links intersecting an entanglement cut to  $I_A$ .

### C. Examples

To be concrete, we discuss the two familiar examples of toric code model and the doubled Fibonacci model.

For the toric code, the input data form the representation category of the  $\mathbb{Z}_2$  group. The label set  $I = \{0, 1\}$ ,  $0* = 0$  and  $1* = 1$ . The quantum dimensions are  $d_0 = d_1 = 1$ , the nonzero fusion rules are  $\delta_{000} = \delta_{011} = \delta_{101} = \delta_{110} = 1$ , with the  $G$  symbols being

$$G_{klm}^{ij} = \delta_{ijm} \delta_{klm^*} \delta_{jkn^*} \delta_{inl}. \quad (17)$$

String-net model outputs four types anyons:  $\{1, e, m, \epsilon = e \oplus m\}$ , where  $e$  is a  $\mathbb{Z}_2$  charge and  $m$  a  $\mathbb{Z}_2$  flux.

There are two Frobenius algebras, i.e. boundary conditions for this input data. One is the trivial  $\mathcal{A}_0 = 0$ , which defines a charge boundary condition. Quasiparticles on the charge boundary are identified with 0 and 1 or equivalently  $\mathbf{1}$  and  $e$ . The other Frobenius algebra is  $\mathcal{A}_1 = 0 \oplus 1$ , with  $I_{\mathcal{A}} = I$ . This is a flux boundary condition. Boundary quasiparticles are identified with  $\mathbf{1}$  and  $m$ . For both types of boundaries, we have

$$\deg_n(\mathbb{Z}_2; D^2) = \binom{L}{n} g_n, \quad g_n(\mathbb{Z}_2; D^2) = 1. \quad (18)$$

This is typical for models with abelian fusion rules.

The simplest non-abelian example is the doubled Fibonacci model, where  $I = \{0, 2\}$  (sometimes also denoted as  $\{1, \tau\}$ ) with  $0* = 0$ ,  $2* = 2$ . Let  $\phi = (1 + \sqrt{5})/2$  be the golden ratio, then the quantum dimensions are given by  $d_0 = 1$  and  $d_2 = \phi$ . The nonzero fusion rules are  $\delta_{000} = \delta_{022} = \delta_{202} = \delta_{220} = \delta_{222} = 1$ , and the independent  $G$  symbols are

$$\begin{aligned} G_{000}^{000} &= 1, \quad G_{022}^{022} = G_{222}^{022} = 1/\phi, \\ G_{222}^{000} &= 1/\sqrt{\phi}, \quad G_{222}^{222} = -1/\phi^2. \end{aligned} \quad (19)$$

The bulk quasiparticles are labeled by  $\{0\bar{0}, 0\bar{2}, 2\bar{0}, 2\bar{2}\}$ , or sometimes  $\{1\bar{1}, 1\bar{\tau}, \tau\bar{1}, \tau\bar{\tau}\}$ . The above input category gives rise to two Frobenius algebras:  $\mathcal{A}_0 = 0$ , which defines a charge boundary condition and  $\mathcal{A}_1 = 0 \oplus 2$ , giving a flux boundary condition. The latter leads to a non-trivial multiplication  $f_{222} = \phi^{-3/4}$ . These two Frobenius algebras are Morita equivalent, i.e. there is a map between all irreducible  $\mathcal{A}_0$  modules and all irreducible  $\mathcal{A}_1$  modules which preserves the fusion rules. Being Morita equivalent to each other means that the two Frobenius algebras give rise to the same boundary condition [17].

The degeneracies are again characterized by  $\deg_n(\text{dFib}, D^2) = \binom{L}{n} g_n(\text{dFib}, D^2)$ , with

$$g_n(\text{dFib}; D^2) = F_{n-1}. \quad (20)$$

Here  $F_n$  the Fibonacci sequence satisfying  $F_1 = F_2 = 1$ ,  $F_n = F_{n-1} + F_{n-2}$  for  $n > 2$ .

## IV. THE CORRESPONDENCE FOR A CYLINDER

### A. Boundary theory on a cylinder

Different boundary conditions or Frobenius algebras  $\mathcal{A}, \mathcal{B}$  can be chosen for the two boundaries  $A$  and  $B$  of a cylinder. In the case without bulk excitations, one can deform the bulk graph by (dual) Pachner moves so that the cylinder graph shrinks to a ring with open links on both sides of the ring, see for example figure 3

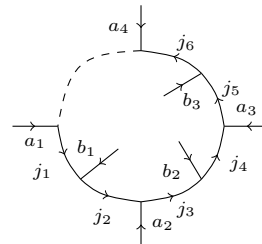


FIG. 3: Effective configuration of on a cylinder.

Both the ground state degeneracy (GSD) and the topological quasiparticles are classified by  $\mathcal{A} - \mathcal{B}$  bimodules. We refer to section 6 of [17] for its detailed mathematical structure.

If both boundaries are simply charge boundaries  $\mathcal{A} = \mathcal{B} = \mathcal{A}_0$ , then the  $\mathcal{A}_0 - \mathcal{A}_0$  bimodule is the entire label set  $I$ , so that both the GSD and the quasiparticles on the cylinder are labeled by the string types  $j \in I$ . Denote the total number of sites as  $L = L_A + L_B$ , and again suppose the charge excitations of type  $\alpha, \beta, \dots, \zeta$  have number  $n_\alpha, n_\beta, \dots, n_\zeta$ , then the degeneracy for the  $n$ -th excited state will be of a familiar form (11), for there is no need to distinguish the two boundaries. But the factor  $g_n$  should now take into account the degenerate ground state subspace on a cylinder. For abelian models this simply amounts to  $g_n = \text{GSD} = |I|$ . For non-abelian cases, the multiple fusion channels and degenerate ground states combine in a nontrivial way. Other kinds of boundaries including the flux type need to be analyzed case by case.

The spectrum becomes more complicated with general combinations of the two boundary conditions. We focus on the toric code model for illustration purpose. There are three possible boundary conditions for the toric code model on a cylinder, labeled by the different Frobenius algebras: (i)  $\mathcal{A} = \mathcal{B} = 0$ , both being charge boundaries; (ii)  $\mathcal{A} = 0$ ,  $\mathcal{B} = 0 \oplus 1$  or  $\mathcal{B} = 0$ ,  $\mathcal{A} = 0 \oplus 1$ , the mixed boundaries; and (iii)  $\mathcal{A} = \mathcal{B} = 0 \oplus 1$ , both being flux boundaries.

Cases (i)(iii) both give twofold GSD, so that

$$\begin{aligned} g_n(\mathbb{Z}_2; \text{cylinder, charge}) &= g_n(\mathbb{Z}_2; \text{cylinder, flux}) \\ &= \begin{cases} 2, & 0 \leq n < L \text{ and } n \in 2\mathbb{Z} \\ 0, & \text{else} \end{cases} \end{aligned} \quad (21)$$

where the  $n \in 2\mathbb{Z}$  constraint arises from the pair creation

of  $\mathbb{Z}_2$  excitations and  $L = L_A + L_B$ . Degeneracy of the  $n$ -th excited state is given by the usual  $\text{deg}_n = g_n \binom{L}{n}$ . By comparison, case (ii) leads to a non-degenerate ground state subspace and

$$g_n(\mathbb{Z}_2; \text{cylinder, mixed}) = \begin{cases} 1, & 0 \leq n < L \\ 0, & \text{else.} \end{cases} \quad (22)$$

The degeneracy of the  $n$ -th excited state is correspondingly

$$\text{deg}_n(\mathbb{Z}_2; \text{cylinder, mixed}) = g_n \sum_{n_A + n_B = n} \binom{L_A}{n_A} \binom{L_B}{n_B}. \quad (23)$$

Intuitively, the above three cases can be understood in terms of the anyon condensation language [28–37]. Case (i) corresponds to the fluxes  $m$  condensing on both boundaries and cannot be distinguished with the vacuum  $\mathbf{1}$ , while the anyons with nontrivial charges  $e$  and  $\epsilon$  becomes excitations on the boundary. So the two GSD correspond to  $\mathbf{1}$  and  $m$ . For case (iii) the GSD is two again, but is now labeled by  $\mathbf{1}$  and  $e$  and correspond to the condensation of  $e$  particles. Then case (ii) is that of the mixed boundaries. The corresponding GSD is only one, since the  $m$  flux can be distinguished from vacuum  $\mathbf{1}$  on the flux boundary, while the  $e$  charge can be distinguished from  $\mathbf{1}$  on the charge boundary. So all four degenerate ground states on the torus can be distinguished on the boundaries. There is no  $n \in 2\mathbb{Z}$  constraint in  $g_n$  in this case, because one can for example create a pair of charges  $e$ , move one of them to boundary  $A$  and the other to  $B$ . On one of these two boundaries,  $e$  is identified with vacuum and thus gives no excitation energy.

We note that the above intuitive understanding helpful but not rigorous; the general relationship between the Frobenius algebra formalism and the anyon condensation picture of boundary theories is yet to be derived.

In a similar fashion, for  $\mathbb{Z}_N$  models we also have case (i) of two charge boundaries and (iii) of two flux boundaries both with  $g_n = N$ , and case (ii) of mixed charge and flux boundaries with  $g_n = 1$ . Additional boundary types other than the charge and flux ones are also possible, giving rise to more combinations.

### B. Entanglement spectrum on a cylinder subsystem

In this section we discuss the entanglement properties of string-net model on a torus, where subsystem  $A$  will have the topology of a cylinder. The focus will be on the abelian  $\mathbb{Z}_N$  models, especially the toric code  $\mathbb{Z}_2$  case.

For toric code model in the quasiparticle basis, a general ground state can be written as  $|\Psi\rangle = c_1 |\mathbf{1}\rangle + c_2 |m\rangle + c_3 |e\rangle + c_4 |\epsilon\rangle$ . Suppose the entanglement cut intersects  $L_A + L_B$  links as in fig. 4, the diagonalized reduced ma-

trix then consists of four blocks

$$\rho_A = 2^{-L_A+1-L_B+1} \begin{pmatrix} |c_1|^2 \mathbb{1} & & & \\ & |c_2|^2 \mathbb{1} & & \\ & & |c_3|^2 \mathbb{1} & \\ & & & |c_4|^2 \mathbb{1} \end{pmatrix}, \quad (24)$$

where each  $\mathbb{1}$  is an identity matrix of dimension  $2^{L_A-1+L_B-1}$ . This is identified with the degeneracies of boundary spectrum on a cylinder from the last section:

$$2^{L_A+L_B} = \sum_{n=0}^{L_A+L_B} \text{deg}_n(\mathbb{Z}_2; \text{cylinder, mixed}). \quad (25)$$

On the entanglement side,  $\text{deg}_n$  is understood as the number of configurations in fig. 3 with altogether  $n$  nontrivial open links that intersect the entanglement cut. The difference factor of 4 between  $2^{L_A+L_B}$  and  $2^{L_A-1+L_B-1}$  gives the topological entanglement entropy, which can be easily read out from the reduced density matrix as

$$S(\mathbb{Z}_2; \text{cylinder}) = (L_A + L_B) \log 2 - 2 \log 2 - \sum_{\mathcal{J}} |c_{\mathcal{J}}|^2 \log |c_{\mathcal{J}}|^2. \quad (26)$$

The first term is the usual area law, while second term arises from the topological entanglement entropy due to the two boundaries of the cylinder as already observed in [20], and the third term is the Shannon entropy from the combination of different  $\mathcal{J}$ 's. For  $\mathbb{Z}_N$  models, this is

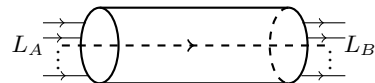


FIG. 4: The entanglement cut generates  $L_A$  and  $L_B$  open links on the two boundaries of the cylinder.

similarly

$$S(\mathbb{Z}_N; \text{cylinder}) = (L_A + L_B) \log N - 2 \log N - \sum_{\mathcal{J}} |c_{\mathcal{J}}|^2 \log |c_{\mathcal{J}}|^2, \quad (27)$$

with  $\mathcal{J}$  running over the  $N^2$  quasiparticles of the  $\mathbb{Z}_N$  model.

From equation (25), we have a correspondence between the cylinder boundary spectrum with mixed boundary condition (22) and the entanglement spectrum. A natural question, then, would be to understand how the other two types of boundaries (i)(iii) can be realized from the entanglement side. To this end, we introduce the simplest graph on a torus given by Fig.5, with three links, two vertices and one plaquette. All other more complicated graphs can be obtained this simplest graph through the (dual) Pachner moves introduced in the first section.

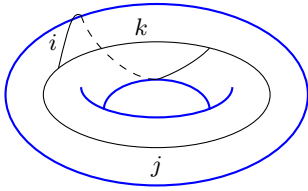


FIG. 5: The simplest graph on torus contains two vertices, three links and one plaquette. Links  $i$  and  $k$  winds the meridian of the torus, while  $j$  and  $k$  winds the longitude.

A general ground state on the simplest graph can be written as a superposition of different configurations  $|ikj\rangle$ . For our toric code example, the relevant states are [41]

$$\begin{aligned}
 |\mathbf{1}\rangle &= \frac{1}{\sqrt{2}}(|000\rangle + |110\rangle), \\
 |m\rangle &= \frac{1}{\sqrt{2}}(|000\rangle - |110\rangle), \\
 |e\rangle &= \frac{1}{\sqrt{2}}(|011\rangle + |101\rangle), \\
 |\epsilon\rangle &= \frac{1}{\sqrt{2}}(|011\rangle - |101\rangle).
 \end{aligned} \tag{28}$$

If the entanglement cut splits the non-contractible loop labeled by  $j$ , for example let  $i, k$  belong to subsystem  $A$  and  $j$  belong to subsystem  $B$ , then  $A$  is topologically a “cylinder” while  $B$  is a “disk”, for there is no non-contractible loop in  $B$ . Then each of these four states (28) gives a trivial reduced density matrix with zero entanglement entropy by itself, due to the small number of total links in this graph. To obtain more general results, we can do dual Pachner moves to complicate the graph, but comply with one important constraint: we want subsystems  $A$  and  $B$  to stay as a cylinder and a disk. Generally the reduced density matrix is [21]

$$\rho_A = 2^{L-1} [(|c_1|^2 + |c_2|^2)\mathbb{1} \oplus (|c_3|^2 + |c_4|^2)\mathbb{1}],$$

with  $\mathbb{1}$  a  $2^{L-1}$ -dimensional identity matrix and  $L$  is the total number of links intersecting the entanglement cut. The entanglement entropy becomes

$$\begin{aligned}
 S(\mathbb{Z}_2, \text{cylinder+disk}) &= L \log 2 - \log 2 \\
 &- \sum_j \left( \sum_{\mathcal{J}} |c_{\mathcal{J}}|^2 M_{\mathcal{J}j} \right) \log \left( \sum_{\mathcal{J}} |c_{\mathcal{J}}|^2 M_{\mathcal{J}j} \right),
 \end{aligned} \tag{29}$$

where the decomposition matrix  $M$  is  $4 \times 2$ -dimensional, with the first subscript taking values from  $\{\mathbf{1}, m, e, \epsilon\}$ , i.e. the output category, and the second subscript from  $\{0, 1\}$ , the input category.<sup>45</sup> Specifically,

$$M_{\mathbf{1}0} = M_{m0} = 1, \quad M_{e1} = M_{\epsilon1} = 1, \quad \text{else} = 0. \tag{30}$$

The rows of  $\mathbf{1}, m$  are exactly the same, so that states  $|\mathbf{1}\rangle$  and  $|m\rangle$  are not distinguishable from the perspective of reduced density matrix. Similar phenomenon happens for the states  $|e\rangle$  and  $|\epsilon\rangle$ : whatever relative weights we

set for these two states, the reduced density matrix and the entanglement entropy are always the same. For this reason, three of the authors generalized the concept of minimally entangled states in [20] to that of the *minimally entangled sectors* [21]. States that cannot be distinguished from the entanglement perspective are understood to be in the same sector. In our example, there are two sectors  $\{|\mathbf{1}\rangle, |m\rangle\}$  and  $\{|e\rangle, |\epsilon\rangle\}$ , which is illustrated in fig. 6. It is possible to reach the maximum entanglement entropy or the minimum topological entanglement entropy only when superposing two ground states  $\mathcal{J}_1$  and  $\mathcal{J}_2$  that come from different sectors.

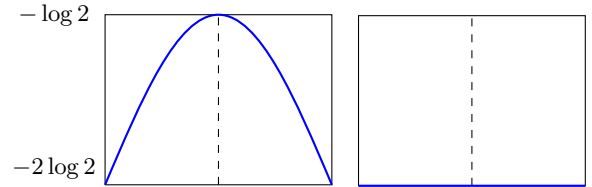


FIG. 6: The entanglement entropy is only sensitive to topological entanglement sectors. The horizontal direction denotes the ratio  $|c_{\mathcal{J}_1}|^2/|c_{\mathcal{J}_2}|^2$ , while the vertical direction is the negative of the topological entanglement entropy. **Left:** superposing ground states in different minimally entangled sectors.  $\mathcal{J}_1$  and  $\mathcal{J}_2$  belong to different sectors (for example one can take  $\mathcal{J}_1 = \mathbf{1}, \mathcal{J}_2 = e$ ). **Right:** superposing ground states in the same minimally entangled sector.  $\mathcal{J}_1$  and  $\mathcal{J}_2$  belong to the same sector (for example one can take  $\mathcal{J}_1 = e, \mathcal{J}_2 = \epsilon$ ).

For  $\mathbb{Z}_N$  models beyond  $N = 2$ , the phenomenon is similar. In the quasiparticle basis, there are  $N^2$  elementary ground states labeled by  $\mathcal{J} = (g, j)$ , with  $g, j \in \{0, 1, \dots, N-1\}$  denoting fluxes and charges, respectively.

$$|(g, j)\rangle = \frac{1}{\sqrt{N}} \sum_{i, k} e^{2\pi i i g / N} \delta_{j i k^*} |i k j\rangle. \tag{31}$$

One observes that the flux and charge degrees of freedom are assigned to the two non-contractible loops  $i$  and  $j$  of the torus (fig. 5), respectively<sup>46</sup>. These states are grouped into  $N$  sectors with the decomposition matrix  $M_{(g, \mu), j} = \delta_{\mu j}$ . Namely, those states that are labeled by the quasiparticles with different fluxes but same charge numbers are in the same sector. In other words, the fluxes are undetectable using entanglement entropy. This is analogous to the situation in the boundary spectrum with two charge boundaries (case i) of toric code discussed in the last section: there the fluxes were also “condensed” and thus undetectable in the energy spectrum. The ground state degeneracy  $N$  on a genuine cylinder is matched with the order of the minimally entanglement sector that contains  $|\mathbf{1}\rangle$ , while  $\text{deg}_n$  on a genuine cylinder is matched to the dimension of the block in the diagonal reduced density matrix that contains  $n$  nontrivial open links. We note that minimally entangled sectors is characteristic of non-chiral topological ordered systems, and is not present in chiral cases [22].

Back to the toric code example, the ground state degeneracy (21) is matched with the order of the minimally entangled sector  $\{|\mathbf{1}\rangle, |m\rangle\}$ , while the excited state degeneracy  $\text{deg}_n$  in (??) is matched with the dimension of the specific block in the reduced density matrix which contains configurations with  $n$  nontrivial open links.

In the above we split  $j$ -loop in the graphs using the entanglement cut and find the correspondence between bulk entanglement and the boundary energy spectra of a cylinder with two charge boundaries (case i). Alternatively, we can split the non-contractible loop labeled by  $i$ . One reads from equation (28) that for the simplest graph, the minimally entangled sectors now change to  $\{|\mathbf{1}\rangle, |e\rangle\}$  and  $\{|m\rangle, |\epsilon\rangle\}$ . As long as one keeps the subsystem  $A$  and  $B$  to be cylinder and disk topologically, one can generate more complicated graphs and obtain the same sectors. This new set of sectors appear as if the charges are invisible to the entanglement spectrum, similar to the ‘‘condensation’’ of charges in the boundary condition (iii) for a genuine cylinder. The ground state degeneracy of the genuine cylinder again matches with the order of the minimally entangled sector which contains  $\mathbf{1}$ , i.e.  $\text{GSD} = |\{|\mathbf{1}\rangle, |e\rangle\}| = 2$ . The story goes in parallel for  $\mathbb{Z}_N$  models. Now the  $N^2$  states are regrouped into  $N$  sectors, and those states whose corresponding quasiparticles have same flux but different charges will be in the same sector.<sup>47</sup>

We summarize the toric code results in the following table I.

Boundary	Bulk Entanglement
(i) charge boundaries	cylinder+disk cut, split $j$ -loop
$\mathcal{A} = \mathcal{B} = 0$ GSD= 2	$\{\mathbf{1}, m\}, \{e, \epsilon\}$ $ \{\mathbf{1}, m\}  = 2$
(ii) mixed boundaries	cylinder+cylinder cut
$\mathcal{A} = 0, \mathcal{B} = 0 \oplus 1$ GSD= 1	$\{\mathbf{1}\}, \{e\}, \{m\}, \{\epsilon\}$ $ \{\mathbf{1}\}  = 1$
(iii) flux boundaries	cylinder+disk cut, , split $i$ -loop
$\mathcal{A} = \mathcal{B} = 0 \oplus 1$ GSD= 2	$\{\mathbf{1}, e\}, \{m, \epsilon\}$ $ \{\mathbf{1}, e\}  = 2$

TABLE I: Summary of the  $\mathbb{Z}_2$  model. The Frobenius algebras  $\mathcal{A}, \mathcal{B}$  specify the boundary conditions of the two boundaries on a cylinder. On a torus there are two non-contractible loops labeled by  $i$  (meridian) and  $j$  (longitudinal). Varying the entanglement cuts changes structure of the reduced density matrix and gives rise to different minimally entangled sectors. (The ‘‘cylinder+disk’’ is a shorthand for taking the subsystems  $A$  and  $B$  to be cylinder and disk, respectively.) Cardinality of the minimally entangled sector that contains state  $\mathbf{1}$  matches with the ground state degeneracy on a cylinder with corresponding boundary conditions. Furthermore, the full entanglement spectrum matches with the boundary excitation spectrum.

## V. DISCUSSION

### A. Non-abelian extension

Section IV has discussed the  $\mathbb{Z}_N$  abelian models on a torus, it would thus be natural to think of a non-abelian version of the correspondence. In this part we study the simplest non-abelian example of doubled Fibonacci model, we will see that the correspondence between boundary ground state degeneracy (GSD) and the order of minimally entangled sector containing  $|\mathbf{1}\rangle$  will need to be generalized.

The basic information of the model was reviewed in III C. Since the two Frobenius algebras  $\mathcal{A}_0$  and  $\mathcal{A}_1$  are Morita equivalent, whichever Frobenius algebras we choose for the two boundaries of the cylinder, the boundary spectrum should be the same. Thus for simplicity, we will focus on the case where  $\mathcal{A} = \mathcal{B} = 0$ , i.e. both boundaries are charge boundaries. Similarly to the  $\mathbb{Z}_N$  case in IV B, this choice corresponds to doing entanglement cut by splitting the  $j$ -loop, and taking the subsystems  $A$  and  $B$  to be cylinder and disk, respectively.

On the side of boundary spectrum, we look at the case of charge boundaries  $\mathcal{A} = \mathcal{B} = 0$ . The degeneracy of  $n$ -th excited state is correspondingly,

$$\text{deg}_n(\text{dFib}; \text{cylinder, charge}) = L_n \binom{L}{n}, \quad (32)$$

with  $L_n$  the Lucas sequence 2, 1, 3, 4, 7, 11,  $\dots$ . The  $n = 0$  case gives the twofold GSD. So we see the GSD is no longer simply matched with the order of the minimally entangled sector containing  $|\mathbf{1}\rangle = |0\bar{0}\rangle$ . A more precise criteria is that *GSD on the boundary = the number of  $\mathcal{J}$  that has nontrivial entry  $M_{\mathcal{J}0} \neq 0$  in the decomposition matrix that appears in the bulk entanglement spectrum*. It reduces to the order of minimally entangled sectors containing  $|\mathbf{1}\rangle = |0\bar{0}\rangle$  for the  $\mathbb{Z}_N$  case. In the doubled Fibonacci example, the two relevant states are  $|0\bar{0}\rangle$  and  $|2\bar{2}\rangle$ . For  $n \geq 1$ , we rewrite  $L_n$  in terms of the Fibonacci sequence  $L_n = 2F_{n-1} + F_n$ , and notice that the first  $F_{n-1}$  term corresponds to the number of channels for fusing  $n$  nontrivial charges to vacuum  $|0\bar{0}\rangle$ , while the remaining  $F_{n-1} + F_n$  corresponds the number of channels for fusing  $n$  nontrivial charges to the other vacuum  $|2\bar{2}\rangle$ .

Next we consider the entanglement properties for a torus. On a simplest graph, the degenerate ground states are

$$\begin{aligned} |0\bar{0}\rangle &= \frac{1}{1 + \phi^2} (|000\rangle + \phi |022\rangle); \\ |0\bar{2}\rangle &= \frac{1}{1 + \phi^2} (|202\rangle + e^{4\pi i/5} |220\rangle - \sqrt{\phi} e^{2\pi i/5} |222\rangle); \\ |2\bar{0}\rangle &= \frac{1}{1 + \phi^2} (|202\rangle - e^{\pi i/5} |220\rangle + \sqrt{\phi} e^{3\pi i/5} |222\rangle); \\ |2\bar{2}\rangle &= \frac{1}{1 + \phi^2} (|000\rangle - \phi^{-1} |022\rangle + |202\rangle + |220\rangle + \phi^{-3/2} |222\rangle). \end{aligned} \quad (33)$$

If the entanglement cut splits the  $j$ -loop, the decomposition matrix is given by

$$M_{0\bar{0},0} = M_{2\bar{2},0} = 1, \quad M_{0\bar{2},1} = M_{2\bar{0},1} = M_{2\bar{2},1} = 1. \quad (34)$$

There are three minimally entangled sectors in this case:  $\mathcal{S}_1 = \{0\bar{0}\}$ ,  $\mathcal{S}_2 = \{0\bar{2}, 2\bar{0}\}$  and  $\mathcal{S}_3 = \{2\bar{2}\}$ . The first two sectors give the following entanglement entropies (where  $L$  is the total number of links intersected by the entanglement cut):

$$\begin{aligned} S_A^{\mathcal{S}_1} &= aL - \log D, \\ S_A^{\mathcal{S}_2} &= aL - \log D + \log \phi. \end{aligned} \quad (35)$$

For the third sector, the reduced density matrix has the structure

$$\rho_A^{\mathcal{S}_3} = \frac{1}{\phi^2} \rho_A^{\mathcal{S}_1} \oplus \frac{1}{\phi} \rho_A^{\mathcal{S}_2}, \quad (36)$$

so that we have

$$S_A^{\mathcal{S}_3} = \frac{1}{\phi^2} S_A^{\mathcal{S}_1} + \frac{1}{\phi} S_A^{\mathcal{S}_2} - \frac{1}{\phi^2} \log \frac{1}{\phi^2} - \frac{1}{\phi} \log \frac{1}{\phi}. \quad (37)$$

For a general state  $|\Psi\rangle = \sum_{\mathcal{J}} c_{\mathcal{J}} |\mathcal{J}\rangle$ , the properties are the following. (i) Superposing states in the same sector does not change the entanglement entropy. (ii) For general superpositions among the three sectors, the maximal topological entanglement entropy is reached when  $|c_{\mathcal{S}_1}|^2 = 1$  and  $|c_{\mathcal{S}_2}|^2 = |c_{\mathcal{S}_3}|^2 = 0$ . Minimal topological entanglement entropy is reached when  $|c_{\mathcal{S}_3}|^2 = 1$  and  $|c_{\mathcal{S}_1}|^2 = |c_{\mathcal{S}_2}|^2 = 0$ . (iii) Specifically, superposing states in sectors  $\mathcal{S}_1$  and  $\mathcal{S}_2$ , and topological entanglement entropy decreases linearly from  $\log D$  to  $\log D - \log \phi$  as  $|c_{\mathcal{S}_2}|^2/|c_{\mathcal{S}_1}|^2$  goes from zero to infinity. (iv) Superposing sectors  $\mathcal{S}_1$  and  $\mathcal{S}_3$ , the topological entanglement entropy again decrease monotonically, from  $\log D$  to  $\log D - (\frac{D}{\phi^2} + \frac{1}{\phi}) \log \phi$  as the weight of  $\mathcal{S}_3$  increases. (v) Similarly, superposing  $\mathcal{S}_2$  and  $\mathcal{S}_3$  leads to monotonically decreasing topological entanglement entropy as the weight of  $\mathcal{S}_3$  increases.

The entanglement spectrum again shares the same degeneracies with the boundary spectrum. The general expression for a cut that splits the  $j$ -loop and separates a cylindrical subsystem  $A$  from a disk  $B$  is<sup>48</sup>, in the language of section III B

$$\rho_A = \sum_{\mathcal{J}} |c_{\mathcal{J}}|^2 \left\{ \bigoplus_{j \in I} M_{\mathcal{J}j} \frac{d_j}{d_{\mathcal{J}}} \left[ \frac{D}{d_j} P_j(\alpha^{\otimes L}) \right] \right\}. \quad (38)$$

In our example, the  $F_{n-1}$  part of (32) comes from  $\rho_{0\bar{0}}$ , while the  $F_{n-1} + F_n$  part arises from  $\rho_{2\bar{2}}$ .

## B. General boundary conditions

We have discussed charge and flux boundary cases, however, for the most general boundary conditions, there are certain limitations and subtleties in the above approach. While the charge boundary always exists, flux boundary may not. This happens in many non-abelian models, for example the doubled Ising case. So letting the entanglement cut split the  $i$ -loop does not always give rise to an entanglement spectrum that correspond to a meaningful boundary spectrum. Additionally, one can have more complicated Frobenius algebras or boundary conditions in addition to these two types. For example, it was shown in Ref. [42] that for the  $\mathbb{Z}_4$  model, there are three different types of boundary conditions, which will lead to six different combinations and thus energy spectra for the two boundaries of a cylinder. It is unclear how one can realize all the corresponding entanglement spectra from the bulk.

The above defects are expected and inevitable because unlike chiral topological orders, in non-chiral cases the boundary-bulk correspondence is many-to-one. The same bulk theory can share many different boundary theories, even gapless ones [44]. Consequently, one cannot extract boundary data purely from bulk information. If one hopes to realize all types of boundary conditions from the entanglement point of view, he/she is forced to add boundaries to the whole system when doing the entanglement calculations. For example, one can start from an cylinder with certain boundary conditions, make a specific bipartition so that the boundaries of both subsystems partially coincide with the boundaries of the manifold (e.g. subsystem  $A$  is a vertical slit of the cylinder that touches both boundaries of the cylinder, and  $B$  is the rest). It was shown in the quantum double case recently [43], that the corresponding entanglement entropy is explicitly dependent on boundary conditions of the cylinder. Within this setup, we expect to be able to distinguish all different boundary conditions from the entanglement spectrum. This strategy, however, unavoidably involves extra input than purely bulk data, and is thus not chosen in this paper.

## Acknowledgments

Zhu-Xi thanks Ling-Yan Hung for helpful discussions.

<sup>1</sup> H. Li and F. D. M. Haldane, Entanglement spectrum as a generalization of entanglement entropy: identification of

topological order in non-Abelian fractional quantum Hall effect states, Phys. Rev. Lett. 101, 010504 (2008).

- <sup>2</sup> F. Pollman, E. Berg, A. M. Turner, M. Oshikawa, Entanglement spectrum of a topological phase in one dimension, *Phys. Rev. B* 81, 064439 (2010).
- <sup>3</sup> L. Fidkowski, Entanglement spectrum of topological insulators and superconductors, *Phys. Rev. Lett.* 104, 130502 (2010).
- <sup>4</sup> A. M. Turner, Y. Zhang and A. Vishwanath, Band topology of insulators via the entanglement spectrum, *Phys. Rev. B* 82, 241102R (2010).
- <sup>5</sup> A. Chandran, M. Hermanns, M. Regnault and B. A. Bernevig, Bulk-edge correspondence in the entanglement spectra, *Phys. Rev. B* 84, 205136 (2011).
- <sup>6</sup> B. Estienne, V. Pasquier, R. Santachiara and D. Serban, Conformal blocks in Virasoro and W theories: duality and the Calogero-Sutherland model, *Nucl. Phys. B* 860 (3), p377-420 (2012).
- <sup>7</sup> J. Dubail, N. Read and E. H. Rezayi, Edge-state inner products and real-space entanglement spectrum of trial quantum Hall states, *Phys. Rev. B* 86, 245310 (2012).
- <sup>8</sup> X.-L. Qi, H. Katsura and A. W. W. Ludwig, General relationship between the entanglement spectrum and the edge state spectrum of topological quantum states, *Phys. Rev. Lett.* 108, 196402 (2012).
- <sup>9</sup> B. Swingle and T. Senthil, Geometric proof of the equality between entanglement and edge spectra, *Phys. Rev. B* 86, 045117 (2012).
- <sup>10</sup> W. W. Ho, L. Cincio, H. Moradi, D. Gaiotto and G. Vidal, Edge-entanglement spectrum correspondence in a nonchiral topological phase and Kramers-Wannier duality, *Phys. Rev. B* 91, 125119 (2015).
- <sup>11</sup> K. Kato and F. G. S. L. Brandão, Locality of edge states and entanglement spectrum from strong subadditivity, arXiv preprint: 1804.05457.
- <sup>12</sup> M. A. Levin and X.-G. Wen, String-net condensation: A physical mechanism for topological phases, *Phys. Rev. B* 71, 045110 (2005).
- <sup>13</sup> S. B. Bravyi and A. Y. Kitaev, Quantum codes on a lattice with boundary, arXiv preprint: quant-ph/9811052.
- <sup>14</sup> B. Salman, P. W. Shor and D. Whalen, The quantum double model with boundary: condensations and symmetries, *Commun. Math. Phys.* 306 (3), p 663-694 (2011).
- <sup>15</sup> A. Kitaev and L. Kong, Models for gapped boundaries and domain walls, *Commun. Math. Phys.* 313, p351-373 (2012).
- <sup>16</sup> T. Lan and X.-G. Wen, Topological quasiparticles and the holographic bulk-edge relation in (2+1)-dimensional string-net models, *Phys. Rev. B* 90, 115119 (2014).
- <sup>17</sup> Y. Hu, Z.-X. Luo, R. Pankovich, Y. Wan and Y.-S. Wu, Boundary Hamiltonian theory for gapped topological phases on an open surface, *JHEP* 1, 134 (2018).
- <sup>18</sup> Y. Hu, Y. Wan and Y.-S. Wu, Boundary Hamiltonian theory for gapped topological orders, *Chin. Phys. Lett.* 34 (7), 077103 (2017).
- <sup>19</sup> M. A. Levin and X.-G. Wen, Detecting topological order in a ground state wave function, *Phys. Rev. Lett.*, 96, 110405 (2006).
- <sup>20</sup> Y. Zhang, T. Grover, A. Turner, M. Oshikawa and A. Vishwanath, Quasi-particle statistics and braiding from ground state entanglement, *Phys. Rev. B* 85, 235151 (2012).
- <sup>21</sup> Z.-X. Luo, Y.-T. Hu and Y.-S. Wu, On quantum entanglement in topological phases on a torus, *Phys. Rev. B* 94, 075126 (2016).
- <sup>22</sup> S. Dong, E. Fradkin, R. G. Leigh and S. Nowling, Topological entanglement entropy in Chern-Simons theories and quantum Hall fluids, *JHEP* 5(2008).
- <sup>23</sup> A. Y. Kitaev, Fault-tolerant quantum computation by anyons, *Annals Phys.* 303, p2-30 (2003).
- <sup>24</sup> P. Etingof, S. Gelaki, D. Nikshych, and V. Ostrik, Tensor categories, *Mathematical surveys and monographs* 205, Providence, Rhode Island : American Mathematical Society (2015).
- <sup>25</sup> S. T. Flammia, A. Hamma, T. L. Hughes and X.-G. Wen, Topological entanglement Renyi entropy and reduced density matrix structure, *Phys. Rev. Lett.* 103, 261601 (2009).
- <sup>26</sup> A. Hamma, R. Ionicioiu and P. Zanardi, Ground state entanglement and geometric entropy in the Kitaev's model, *Phys. Lett. A* 337, 22 (2005).
- <sup>27</sup> A. Hamma, R. Ionicioiu and P. Zanardi, Bipartite entanglement and entropic boundary law in lattice spin systems, *Phys. Rev. A* 71, 022315 (2005).
- <sup>28</sup> T. Lan, J. Wang and X.-G. Wen, Gapped domain walls, gapped boundaries, and topological degeneracy, *Phys. Rev. Lett.* 114, 076402 (2015).
- <sup>29</sup> F. A. Bais, B. J. Schroers and J. K. Slingerland, Broken quantum symmetry and confinement phases in planar physics, *Phys. Rev. Lett.* 89, 181601 (2002).
- <sup>30</sup> F. A. Bais, B. J. Schroers and J. K. Slingerland, Hopf symmetry breaking and confinement in (2+1)-dimensional gauge theory, *JHEP* 05 (2003).
- <sup>31</sup> F. A. Bais and J. K. Slingerland, Condensate-induced transitions between topologically ordered phases, *Phys. Rev. B* 79, 045316 (2009).
- <sup>32</sup> L.-Y. Hung and Y. Wan, Ground-state degeneracy of topological phases on open surfaces, *Phys. Rev. Lett.* 114, 076401 (2015).
- <sup>33</sup> A. Kapustin and N. Saulina, Topological boundary conditions in abelian Chern-Simons theory, *Nucl. Phys. B* 845, p393-435 (2011).
- <sup>34</sup> M. Levin, Protected edge modes without symmetry, *Phys. Rev. X* 3, 021009 (2013).
- <sup>35</sup> M. Barkeshli, C.-M. Jian and X.-L. Qi, Theory of defects in abelian topological states, *Phys. Rev. B* 88, 235103 (2013).
- <sup>36</sup> L. Kong, Anyon condensation and tensor categories, *Nucl. Phys. B* 886, p436-482 (2014).
- <sup>37</sup> T. Neupert, H. He, C. von Keyserlingk, G. Sierra and B. A. Bernevig, Boson condensation in topologically ordered quantum liquids, *Phys. Rev. B* 93, 115103 (2016).
- <sup>38</sup> U. Pachner, P. L. Homeomorphic manifolds are equivalent by elementary shellings, *Europ. J. Combinatorics* 12, p129-145 (1991).
- <sup>39</sup> Y. Hu, N. Geer and Y.-S. Wu, Full dyon excitation spectrum in generalized Levin-Wen models, arXiv preprint: 1502.03433.
- <sup>40</sup> H. Yao and X.-L. Qi, Entanglement entropy and entanglement spectrum of the Kitaev model, *Phys. Rev. Lett.*, 105, 080501 (2010).
- <sup>41</sup> Yu-Ting Hu, Emergent properties in exactly solvable discrete models for two-dimensional topological phases, Thesis, University of Utah.
- <sup>42</sup> J. C. Wang and X.-G. Wen, Boundary degeneracy of topological order, *Phys. Rev. B* 91, 125124 (2015).
- <sup>43</sup> C. Che, L.-Y. Hung, Y. Li, and Y. Wan, Entanglement entropy of topological orders with boundaries, arXiv preprint: 1804.05725.
- <sup>44</sup> L. Kong and H. Zheng, Gapless edges of 2d topological orders and enriched monoidal categories, *Nucl. Phys. B* 927, 140-165 (2018).
- <sup>45</sup> The decomposition  $M$  similar to but different from the tunneling matrix introduced in [28] in the range and meaning

of the second subscript. For details see [21].

<sup>46</sup> We have used the bold  $\mathbf{i}$  to denote the imaginary unit, in order to distinguish it from the link  $i$ . The phase factor  $e^{2\pi i \mathbf{i} g/N}$  is the half braiding tensor in the sense of [12,39]. For the  $\mathbb{Z}_N$  case it translates the flux degree of freedom  $g$  to link degree of freedom  $i$ .

<sup>47</sup> If the cut splits the  $i$ -loop, entanglement entropy will have an additional term of  $\log D = \log N$  due to the Fourier transform between flux degrees of freedom  $g$  and the string types  $i$  in (31).

<sup>48</sup> (38) is the case  $L_1 = L, L_2 = 1$  in Ref. [21]